# Seahorse Bone Structure Offers Inspiration for Robot Development

Michael Gilroy, Katrina Arbogast, Pravesh Rana, Ismail Hussein, and Diego Guzman
*Department of Mechanical Engineering*
*University of Colorado*
Boulder, Colorado, United States

## Abstract

Seahorses have long attracted much scientific interest due to their many distinct features, including their equine-like appearance, vertical swimming position, camouflage abilities, and prehensile tail. In this work we build off several studies into the skeletal structure of the seahorse tail, which is unique in its ability to bend and undergo compression while its outer "armor" of overlapping bony plates provides protection against crushing by predators. Our objective was to enhance a kirigami-based hexapod robot by incorporating a modified central skeletal structure that mimics the bone structure of the seahorse tail, with the goal of increasing the robot's flexibility, compressibility, and maneuverability. Using modern additive manufacturing capabilities, we developed a novel body structure for our robot now referred to as the Seahorse Kinetic Interlocking Plate System (SKIPS), which emulates the structure, flexibility, and compressibility of the seahorse tail. Future iterations of SKIPS could have applications in robots for search and rescue and undersea exploration, as well as in designing disaster-resistant structures.

## I. Introduction

A fundamental property of many living organisms is their ability to move themselves through their environment. Those interested in the natural world have long been intrigued by the wide variety of body structures and methods of locomotion among living creatures. As robotic technology expands, many in the field are increasingly looking at the motion of animals to inspire development of novel designs. Here we take inspiration from seahorses of the genus *Hippocampus* in developing a robot body structure that is uniquely flexible and deformable.

Our team of science and engineering students at the University of Colorado, Boulder, has previously done work building a kirigami-based robot whose locomotion was inspired by that of a hexapod insect. The design was based off the Dynamic Autonomous Sprawled Hexapod (DASH) robot, developed by DASH Robotics Inc. We extended the functionality of the DASH robot by implementing tactile sensors inspired by insect antennae to detect and avoid obstacles in its path. In our recent work, described here, we looked beyond hexapod insects for bioinspiration in expanding our robot's motion capabilities.

One organism that we studied is the centipede, which has a flexible body structure consisting of numerous segments and legs. Centipedes move in a unique pattern of locomotion with body undulations which are absent at low walking speeds, but appear at higher speeds with increasing amplitude and wavelength as speed increases. Research documented in [1] suggests that these body undulations may be a passive byproduct of the way the centipede's muscles move during faster locomotion, but the underlying mechanism is still unclear. Another organism we looked at is the tobacco hornworm or *Manduca sexta*, a species of caterpillar. Caterpillars have a segmented body structure similar to centipedes and some other invertebrates, but have a unique manner of crawling where anterior segments crawl forward first and extend the body, after which posterior segments catch up. A recent study into the hornworm's motion supports a tension-based model of propulsion where contraction of the muscles in the anterior segments generates tension between the anchored posterior segments which then pulls those segments forward [2].

We also examined various features of sea creatures, many of which have unique locomotion as well as structural components that help them resist crushing by predators [3], [4]. The seahorse specifically captured our attention because of its distinctive skeletal structure, seen in Fig. 1. While most fish, crustaceans, and mollusks have scales, shells, or exoskeletons that serve as armor against predators and their environment, seahorses have a subdermal skeleton consisting of overlapping segments of bony plates [3], [4]. The tail of the seahorse is especially unique as unlike most fish, it can bend ventrally, compress by up to 50 percent in all three orthogonal directions, and exhibits prehensile properties [4], [5].

Several studies documented in [3] - [5] have helped uncover more details of the seahorse's skeletal structure. The structure of the seahorse tail consists of articulating segments with square cross sections, each consisting of four overlapping bony plates surrounding a central vertebrae, as shown in Fig. 2. A combination of sliding and ball-in-socket joints allow for relative motion between the bony plates, both within each square segment and between segments [3], [4]. Meanwhile, the outer plates are connected to the central vertebrae by internal struts that can elastically buckle, allowing for compression without permanent damage [4]. In-depth analysis of seahorses' vertebrae structure and muscle activity in [5] has shown that its unique flexibility and prehensile properties are largely enabled by its distinct skeletal structure. Testing documented in [6] also found that the square cross-sectional shape of the seahorse tail helps it perform better in prehension and resistance to crushing

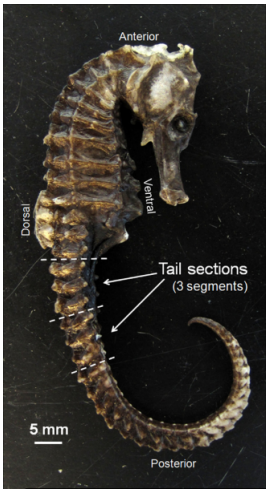


Fig. 1. Skeletal structure of spotted seahorse, *Hippocampus kuda* [4]

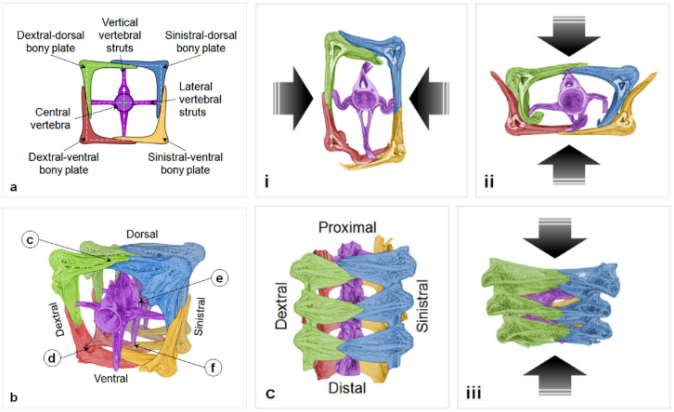


Fig. 2. Schematic of seahorse tail cross-section and manner of compression, based on the work of Porter et al. [4]

versus a circular cross section which is more commonly found in animal tails.

One of the aforementioned studies is a 2012 study into seahorse bone structure by Porter et al. [4] which provided the primary bioinspiration for our robot. In this study, several tail segments of spotted seahorses, *Hippocampus kuda*, were deproteinized, electronically imaged, and tested for material composition, microhardness, and compressibility. Appendix A provides a full summary and analysis of the study in [4] in the form of a discovery decomposition flowchart.

Among the key findings of [4] was that both the material composition of the tail's bony plates as well as their shape and arrangement appear to play a significant role in the flexibility and compressibility properties of the seahorse. The material composition of the bones is a combination of organic material, minerals, and water that makes them deformable and energy absorbent while still having a hard exterior. Meanwhile, the grooves of the internal joints are softer, allowing for more motion between the plates and segments. At the same time, the previously-described structure and arrangement of the bones allow for significant displacement and relative motion during tail bending and compression without incurring permanent damage [4].

Inspired by research in [3] - [6], we developed a novel central body structure for our hexapod robot, which we called the Seahorse Kinematic Interlocking Plate System (SKIPS). The goal in developing SKIPS was to create a robot body modeled after the skeletal structure of the seahorse tail to partially mimic its flexibility and compressibility. In doing so, we hoped to create a robot that could more easily maneuver through constrained spaces and would be more resilient against potential damage. The primary focus was on mimicking the structure and arrangement of the seahorse tail skeleton, while secondary focus was given to material properties due to constraints on material and manufacturing options. The kirigami legs and electronic system were adapted from our previously-developed hexapod robot to accommodate the new skeletal structure. Appendix A provides an analogy table with a full comparison of the robot design to the seahorse tail structure it is modeled after. The following sections provide full details on the design, fabrication, electronic control, and testing of the SKIPS robot.

## II. Design and Fabrication

### A. Central Body Skeleton

Our primary design goal for the robot skeleton was to model its structure after the structure of the seahorse tail skeleton to mimic the tail's flexibility and compressibility. Additionally, while it was impossible to match the material properties of the seahorse bones, we wanted to use materials that would enable similar manners of motion within and between segments.

As seen in the Fig. 2 schematic taken from [4], the tail structure is comprised of articulating segments with a square cross-section. Each segment has four outer overlapping L-shaped plates surrounding an internal spine with four lateral struts connecting to the outer plates. The spine bends significantly during tail bending and its struts buckle during compression, while the outer plates largely maintain their L-shape as they slide past each other during tail deformation. To mimic this structure, we used SolidWorks to design similar body segments for our robot with simplified geometry. Each segment consisted of an internal spine with four protruding struts, surrounded by four overlapping L-shaped plates. The outer plates were 3D printed using polylactic acid (PLA) to make them rigid, while the inner spine was 3D printed using NinjaFlex thermoplastic polyurethane (TPU) to make it somewhat flexible and elastic. Rubber band segments were used to attach the overlapping pairs of plates together and connect them to the ends of the struts, allowing the overlapping plates to slide past each other during compression but returning them to their original configuration when compression forces were released.

Fig. 3(a) shows our initial concept for the robot body, modeled in SolidWorks. While the seahorse tail consists of 36 segments that decrease in size down the tail, allowing it

to bend over 360 degrees, our initial design goal was only 15 degrees of bending. We thus designed our initial concept to have five identical segments, to simplify manufacturing and meet time constraints. However, we were unable to mount legs on both sides of the segments as shown in Fig. 3(a), since on one side the bottom plate would become covered by the top plate during compression. We thus changed our design to have six segments alternating in directions of overlap as shown in Fig. 4 , such that the six legs could be mounted alternately on each side.

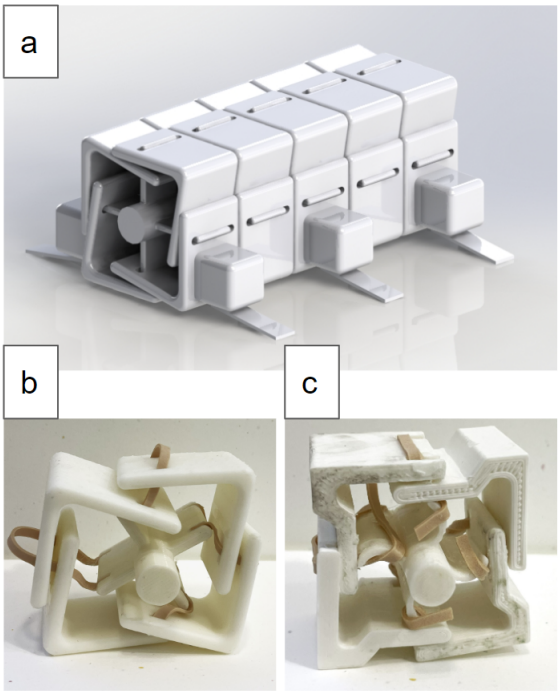


Fig. 3. (a) Initial concept for robot body, modeled in CAD; (b) initial prototype of body segment; (c) second iteration of body segment

Fig. 3(b) shows the initial prototype of one of the body segments. Like the seahorse body segments, the internal spine had four straight struts connecting it to the outer plates. These struts were intended to buckle under compression, but due to their stiffness the spine instead rotated out of position when the segment was compressed. Additionally, the L-shaped plates did not slide past each other cleanly, limiting compressibility.

The second iteration of the body segment is seen in Fig. 3(c). The struts on the inner spine were made thinner and crescent-shaped to facilitate buckling. The shape of the outer plates was also modified to improve their ability to slide over each other. Notches were added in each plate for the adjacent plate to slide into, increasing the room for potential compression.

Our final segment and body design is design is shown in Fig. 4. As seen in Fig. 4(a), the segment design was similar to the second iteration, but the outer plate thickness was reduced from 4 to 3 millimeters to reduce weight and increase room for compression. The crescent shape of internal struts was also

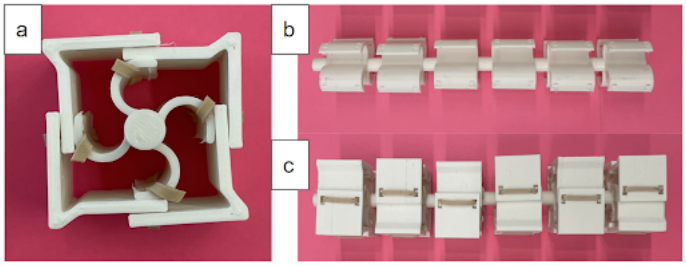


Fig. 4. (a) Final segment prototype; (b) final internal spine prototype; (c) final assembled robot skeleton

further exaggerated to improve buckling. SolidWorks models of the final design are available in Appendix B.

Fig. 4(b) and (c) show the assembled inner spine and final assembled skeleton, respectively. The fabrication process consisted of first 3D printing the outer plates and internal spine segments from PLA and NinjaFlex, respectively. Each segment was then individually assembled by first supergluing the inner spine struts to two opposite outer plates. The remaining plates were then put in place, and rubber band segments were thread through the overlapping plates and glued to the connecting struts. After assembling the individual segments, the spine ends of adjacent segments were glued together such that consecutive segments alternate in direction of plate overlap, as shown in Fig. 4(c). We originally planned to run a thick cord through the center of the spine to hold the segments together, but this proved to be unnecessary as superglue was strong enough to keep the segments connected even under intense bending of the structure.

Our planned final design also included peg-socket linkages between the body segments, as shown in Fig. 5. These peg-socket joints were modeled after similar joints on the seahorse skeleton, and would provide several advantages in skeletal strength and performance if implemented on the robot body. Peg-socket linkages would prevent extreme torsion and lateral bending between individual segments which could lead to failure of the structure. They would also increase the shear stress threshold of the system significantly and distribute forces acting on a single segment to adjacent segments, increasing overall body strength. While these peg-socket joints were not implemented due to poor printer accuracy and time constraints, they would be an obvious first step for any future work.

### *B. Leg Modules and Motor Mounting*

In addition to the central skeletal structure, the SKIPS robot design also included functions for terrestrial locomotion with six individually fabricated and controlled legs. In previous iterations of the DASH V2 robot, the hexapod gait was controlled by legs that were linked together mechanically on either side of the frame. Given the flexible and compressible nature of SKIPS, our design required a leg system that allowed for lateral flexion. To this end, we used the kirigami-based Single Leg Design Clari-Mega Leg Module 1 designed previously by colleague Riley McGill, as seen in Fig. 6. McGill's design was used in its original form, except for the addition of extra layers

Fig. 5. CAD model of final body design with peg-socket linkages added between segments

of material to increase leg strength. Sandpaper was also added to the bottom of the legs, as shown in Fig. 6(c), to improve traction on smooth surfaces, and toothpick segments were later added to the cross bars to mitigate bending.

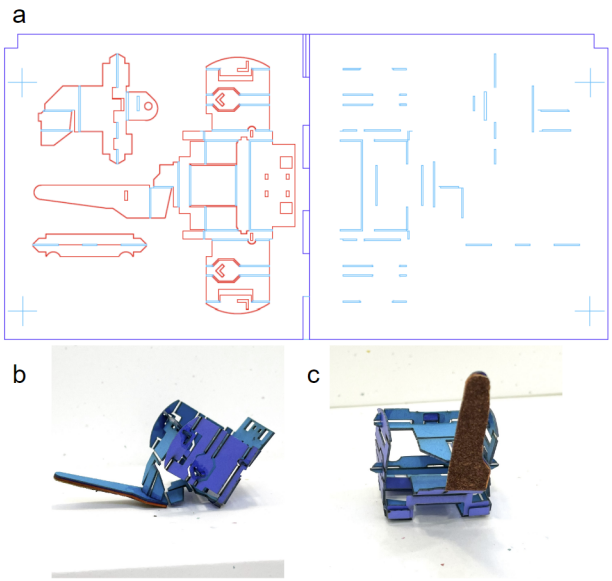


Fig. 6. (a) Autocad design for laser cutting of Single Leg Design Clari-Mega Leg Module 1; (b) side view of single-leg module; (c) bottom view of single-leg module

The single-leg modules were constructed using stack-laminate fabrication and kirigami folding techniques. The main structure of the leg module is made out of seven laminated layers of materials, in the order: card paper - adhesive - plastic sheet - adhesive - card paper - adhesive - card paper. The foot then has eight additional layers for strength and friction, added to the bottom in the order: superglue - card paper - adhesive - card paper - adhesive - card paper - superglue - 80 grit sandpaper. The laser machining process for the leg module has two main steps; the first step cuts out the areas where the plastic sheet will be used as joints, and the second is the final cut around the outside of the module pieces. In Fig. 6(a) the blue represents the joint cuts and red represents the final cuts. Once cut out, the three individual pieces were connected using superglue to form the three dimensional module shown in Fig. 6(b) and (c). During testing the strain of movement also caused bending in the cross bar connecting the frame of the leg to the linkage system, so toothpick segments were added using superglue to reduce this bending.

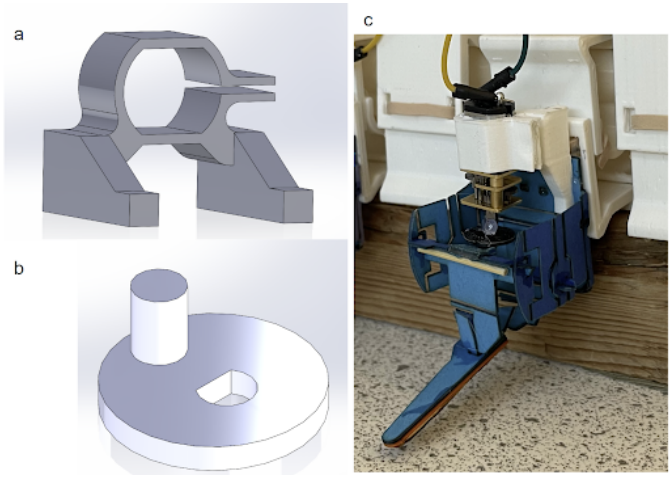


Fig. 7. (a) CAD model of motor mount; (b) CAD model of motor-to-leg linkage disc; (c) 3D-printed mount and linkage disc with motor installed on leg module

The motors were attached to the leg modules using custom motor mounts and circular linkage discs. Fig. 7(a) and (b) show CAD models of the mount and disc, respectively, which are also available in Appendix B. The mounts were based on previous motor mounts designed for the DASH V2 robot, since the motors used were the same; however, the legs of the mount were extended to position the motor properly, and support flanges were added to the structure. The linkage discs were designed to translate rotational motion from the motor shaft to the connecting hole on the leg linkage, and were sized based on the rotation radius of the leg linkage. Both components were designed in SolidWorks and 3D printed using PLA. Fig. 7(c) shows one of the leg modules with its motor attached using a printed mount and disc.

## III. Control

Fig. 8 shows a wiring diagram of the robot's electronic system. The robot was controlled by an Arduino Nano micro-controller and was powered off a rechargeable USB power bank that sits on the robot. A soldered circuit board on the robot was used to connect the wires from the electronic components. Details on the electronic components and the Arduino code used to interface with them are given in the following sections. The complete Arduino code is provided in Appendix C.

### A. Motor Control

Six geared DC motors were used to independently actuate each of the robot's six legs. The motors had a 298:1 gearing

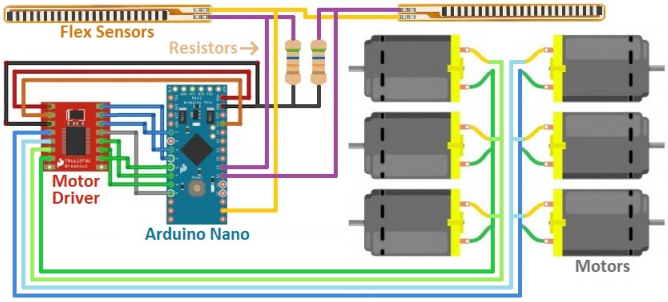


Fig. 8. Wiring diagram of robot's electronics

ratio, making them high in torque and low in speed. Initially, we tried using lightweight non-geared DC motors to minimize the motors' weight on the robot; however, these motors failed to provide sufficient torque to consistently actuate the legs even without supporting the robot's weight, so we replaced them with higher-torque geared motors.

In previous versions of the DASH robot, the three legs on each side were mechanically linked, with the middle leg offset 180 degrees in its rotation cycle from the front and rear legs in order to replicate the "alternating tripod" manner of locomotion of a hexapod insect. The SKIPS robot was designed to have the same manner of locomotion; however, the flexibility of its body made it difficult to mechanically link the legs. Instead, the three legs on each side of the robot were electrically connected, such that they all received the same signals. The middle leg on each side was manually set to a 180 degree offset from the front and rear legs. Minor differences in the rotation speeds of the motors made it necessary to periodically resynchronize the motor rotation cycles.

A TB6612FNG motor driver was used to regulate power to the motors. The motor driver was connected to the motors and Arduino as shown in Fig. 8. The Arduino code controlled the motors using five functions for the five directions of motion—forward, reverse, left turn, right turn, and stop. When a function was called, the Arduino sent the appropriate signals to the motor driver. For each grouping of three motors, two digital pins on the Arduino were used to communicate the desired direction of rotation to the motor driver, while a third digital pin was used to send a pulse-width modulated (PWM) signal to the driver indicating the desired motor speed. The motor driver then powered each grouping of motors as appropriate given the requested direction and speed. Power was drawn from the Arduino's VIN pin which connects directly to the 5 volt power bank.

### B. Antenna-Inspired Sensors

To add to the robot's functionality, two Spectra Symbol flex sensors were mounted on the front of the robot as shown in Fig. 9. These sensors were intended to mimic the functionality of insect antennae, which are used in part to detect obstacles in the insect's path of motion. Fig. 8 shows the wiring of the sensors to the Arduino. These variable-resistance sensors increase in resistance as they are flexed, from 10 kilohms when flat up to 30 to 40 kilohms when bent to 90 degrees. Each sensor was wired in series with a 100 kilohm resistor to form a voltage divider as shown in Fig. 10. The output voltage, measured by the Arduino's analog input pins, could then be used to determine the change in resistance of the sensor from flexing, according to the formula

$$V_{out} = V_{in} \frac{R_2}{R_1 + R_2} \tag{1}$$

where $R_1$ is the sensor resistance and $R_2$ is the resistance of the static resistor, 100 kilohms. A change in output voltage beyond a certain threshold indicated that the corresponding sensor had been flexed backward by an obstacle encountered on that side of the robot. The Arduino program would respond by turning the robot in the opposite direction until the obstacle was no longer detected by the sensor, indicating that the robot was free to proceed forward.

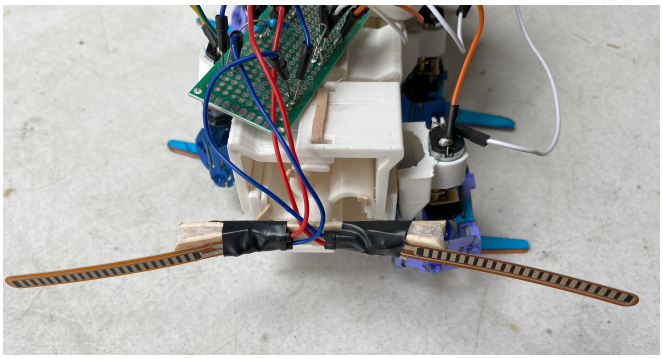

Fig. 9. Flex sensors mounted on front of robot

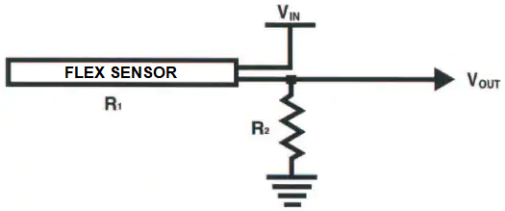


Fig. 10. Voltage divider circuit used to implement flex sensors

### C. Bluetooth Control

The final objective of the Arduino code was to enable remote control of the robot using a smartphone. To accomplish this, the robot was coded to interface with the LightBlue smartphone app using Bluetooth Low Energy (BLE). This code was partially taken from a tutorial on the Arduino website [7]. Once connected to the Arduino, eight different numerical commands could be sent from the LightBlue app to the Arduino, corresponding to the five directions of robot motion and three different motor speeds. When a command was received by the Arduino, the code would interpret the command and call the appropriate motor function.

## IV. Testing

To test SKIPS robot skeleton against our design goals, we performed compressibility, flexibility and maneuverability tests. In order to test the maximum capabilities of the SKIPS structure, these tests were performed without the legs or electronics attached. Fig. 11 shows schematics of how these three tests were performed.

Additionally, once the legs and electronics were attached, the complete robot was tested in its ability to move across the surface, and results were compared to the previous iteration of the DASH V2 robot. The flex sensors were also tested in their ability to detect obstacles and adjust the robot's motion accordingly. All test videos can be found in Appendix D.

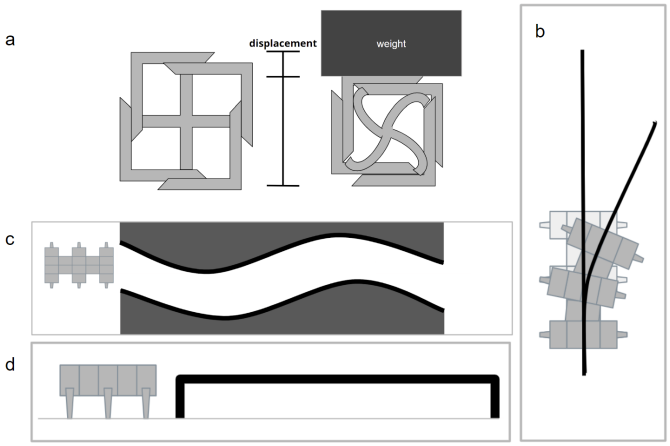


Fig. 11. Testing set up schematics for (a) compression test; (b) flexibility test; (c) and (d) maneuverability test

### A. Compressibility Test

Compressibility testing was performed on a singular body module to determine the amount of compression that occurs when varying weights are placed on top of the module. As the module is symmetrical, the module could be oriented in any direction for similar results. The height of the uncompressed module is 50 millimeters, as seen in Fig. 12(a), and its height under compression is measured using electronic calipers as shown in Fig. 12(b). The maximum compression of the module, restrained using elastic cords, is shown in Fig. 12(c). Compression test results are given in Table I.

TABLE I
Compression Test Results

| Weight on Module (g) | Resulting Module Height (mm) | Compression Distance (mm) | Compression Percent |
|---|---|---|---|
| 0 | 50.0 | 0.0 | 0.0 |
| 100 | 50.0 | 0.0 | 0.0 |
| 500 | 48.0 | 2.0 | 4.0 |
| 1000 | 44.9 | 5.1 | 10.2 |
| Max Comp. | 38.3 | 11.7 | 23.4 |

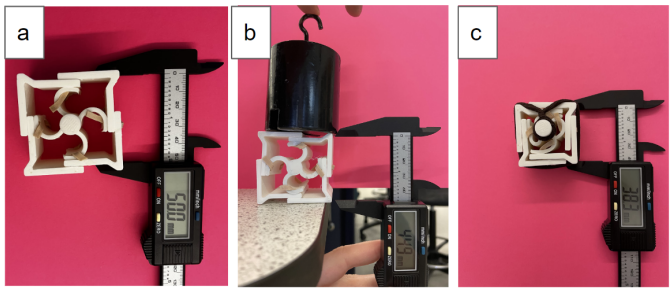


Fig. 12. (a) Relaxed module; (b) module compressed under 1000 g weight; (c) module at maximum compression

### B. Flexibility Test

Flexibility testing was performed to determine the amount of lateral bending the SKIPS structure can undergo, as shown in Fig 13. Two sets of tests, one on the inner spine and another on the fully assembled structure, were performed to understand the extent to which the outer plate structure affected flexibility. The spine's radius of curvature and the internal arc angle at maximum bending were measured and are given in Table II.

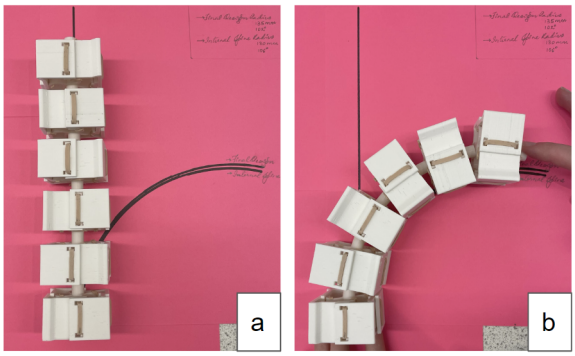


Fig. 13. Flexibility test of SKIPS, showing (a) relaxed state and (b) maximum bending

TABLE II
Flexibility Test Results

| Structure Tested | Radius of Curvature (mm) | Internal Arc Angle (°) |
|---|---|---|
| Internal Spine | 130 | 106 |
| Full Structure | 135 | 102 |

### C. Maneuverability Test

Maneuverability testing was performed to assess the SKIPS structure's ability to traverse through a curved acrylic track. The track, shown in Fig. 14, is 914 millimeters long, while the curves have a central circular radius of 240 millimeters. Based on the 240-millimeter length of the SKIPS body, these curves would bend the body to 57 degrees, which is a little over half the maximum curvature measured in the flexibility test. For testing, the body is mounted on two sets of dowel axle pairs with attached wooden wheels to reduce friction

with the ground. The acrylic track is raised above the floor using wooden blocks, such that it does not interfere with the wheels while still restricting the main body's movement. The body is then pulled through the track by a string, forcing it to flex around the curves. Throughout multiple trials, the SKIPS structure consistently maneuvered through the track successfully.

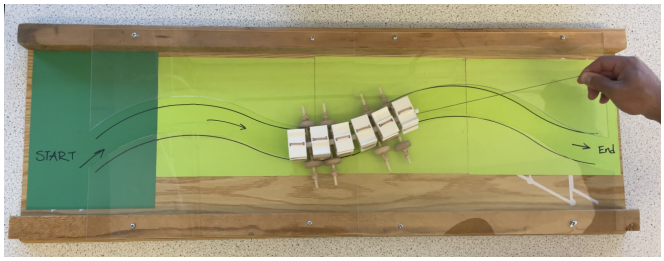


Fig. 14. Maneuverability test setup using curved acrylic track

### D. Motion and Sensor Testing

Our final assembled robot, with legs and electronics connected, is shown in Fig. 15. Appendix D includes videos showing motion and sensor testing on the completed robot. While the electronics, smartphone control, and sensors all worked as intended, the robot's ability to move forward was minimal—far underperforming the previous DASH V2 robot in its walking speed. This was because the weight of the body—even with the breadboard and power bank removed—was too heavy for the design of the legs. While the legs were able to hold up the robot's weight, they were pushed flat against the ground instead of contacting the ground only at their outermost point as is intended for locomotion.

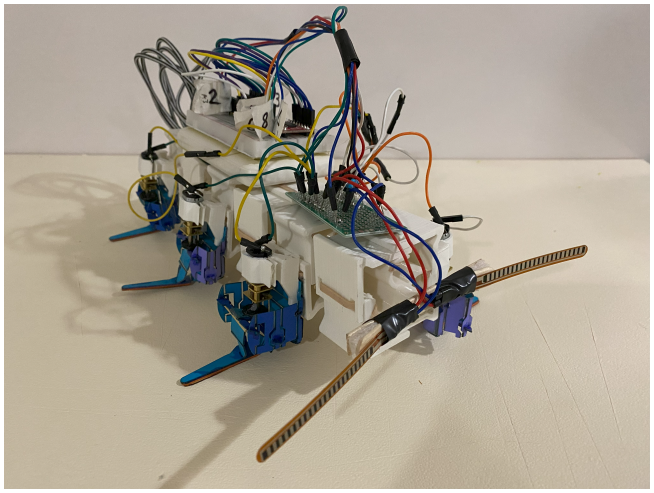

Fig. 15. Final assembled robot

## V. Discussion

In evaluating the performance of the SKIPS body structure as well as the completed robot, it is useful to consider both design goals as well as the performance of the seahorse tail structure that inspired our design. Manufacturing limitations prevented us from accurately replicating the material properties of the seahorse bones and forced us to simplify their shape and structure in our model; nevertheless, we hoped to at least partially replicate the flexibility and compressibility of the seahorse tail.

Regarding compressibility, the seahorse tail skeleton can be compressed without permanent deformation by up to 50 percent in all three orthogonal directions. Our design goal was 30 percent compression in the two directions orthogonal to the spine, as we did not design for compression along the length of the spine. The compression test revealed a maximum compressibility of our design by up to 23.4 percent in these two orthogonal directions, falling short of our design goal. Nonetheless, achieving a lateral compression nearly half that of the seahorse skeleton, given our design and manufacturing limitations, was still a success.

For flexibility, the seahorse tail can bend up to around 360 degrees over its 36-segment length. Our initial design goal was 15 degrees of bending, but we later increased this to 60 degrees to match the 10-degree-per-segment bending of the seahorse tail. The SKIPS body structure greatly exceeded this goal with 102 degrees of bending in the flexibility test. It is worth noting, however, that the structure achieved this without the peg-socket joints connecting the outside edges of adjoining body segments, which the seahorse skeleton has and which we planned to include in our design. These joints would likely partially restrict bending, but have other benefits in improving the strength and durability of the skeletal structure.

Regarding maneuverability, we had no way of quantifying the seahorse's performance, but hoped to design a body structure that could maneuver a curved test course that the rigid DASH V2 robot would be unable to navigate. Our curved maneuverability test course was designed to be too curvy and narrow for the dash robot, and the SKIPS body structure did successfully maneuver through it. However, while we hoped for the completed robot to autonomously attempt the course with its legs and electronics connected, its failure to move prevented that test from occurring.

Actual locomotion is indeed where are robot fell short, relative to both the previous DASH V2 robot and our expectations. The robot's inability to generate significant forward motion was a result of the body structure being too heavy for the leg design, forcing the legs to lay flat against the ground instead of standing on their tips. However, the electronics, Bluetooth control, and sensors all worked as intended and actuated the legs in the expected manner. Furthermore, our previous work with the Dash V2 robot showed that we can successfully implement both remote control and autonomous sensor-aided navigation.

## VI. Conclusion

Our work with bioinspired robotics thus far has shown the great potential for biomimicry in the field of robotics. By studying the structures and behaviors of natural organisms, we may develop robots that are more adaptable and efficient

in their tasks and environments. The Seahorse Kinetic Interlocking Plate System (SKIPS) presented in this paper is a step forward in this direction, demonstrating the ability to create a flexible and compressible design inspired by nature—in this case, the structure of a seahorse tail.

Our design for SKIPS was inspired by several distinctive features of the seahorse tail, including its structure, arrangement of bones, and the combination of hard exterior plates with a soft interior spine. Fig. 16 shows the similarities and differences in our design compared to the organic design of a seahorse skeleton. The differences arose in part due to our different design goals and operating environment—the seahorse is a fish that swims in water with an upright posture and needs to protect itself against predators, while our robot is terrestrial and crawls parallel to its spine with hexapod-inspired locomotion. Additionally, some differences were mandated by our limitations in materials, manufacturing methods, budget, and time. It is most important, though, to point out the similarities of the hard exterior plates that form a square cross section as seen in Fig. 16(b)-(d). The interlocking plates, central deformable spine, and their overall arrangement are similar between the bone structure of the seahorse and the model of SKIPS, providing exceptional strength and resilience, while simultaneously allowing elastic deformation in response to external forces or to maneuver through the environment.

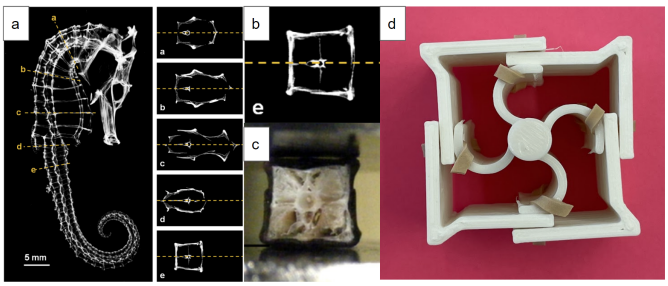


Fig. 16. Comparison of seahorse tail segment [4] and SKIPS segment: (a) Micro CT scan of a juvenile seahorse skeleton (*Hippocampus kuda*) illustrating the cross-sections of several different segments along the length of the fish; (b) zoomed in image of (a) looking at the cross section of the tail segment; (c) preserved skeleton segment from a Hippocampus kuda [4]; (d) cross-section photo of final design of SKIPS body segment

While the motion capabilities of the robot were disappointing, the development and performance of the SKIPS structure can be considered a success. The body structure was able to at least partially replicate the compressibility and flexibility of the seahorse tail structure it was modeled after, as well as maneuver through a tight curved test track. In developing the robot, we combined kirigami and stack-laminate fabrication techniques with additive manufacturing, and were able to successfully implement bioinspired sensors and control the robot remotely from a smartphone.

Future work will focus on finding stronger materials from which to manufacture the robot legs, or pursuing a more robust leg design altogether, as well as perhaps finding lighter-weight 3D-printable materials for the robot structure. We also hope to further iterate the body design to improve performance, including by adding peg-socket joints between the body segments as modeled after the seahorse structure to increase strength and durability. Our hope is to eventually see the SKIPS body design incorporated into a fully functioning robot to truly evaluate its performance and functionality as a robot structure. We believe the SKIPS structure could have applications on robots that need to navigate tight spaces or resist damage from unstable environments, such as those designed for disaster recovery, search and rescue, or undersea or extraterrestrial exploration. The seahorse-inspired design may also be useful in making vehicles safer and more resilient in crashes, or designing structures to withstand natural disasters.

## APPENDIX A

The discovery decomposition flowchart for "Highly deformable bones: Unusual deformation mechanisms of seahorse armor" [4], as well as the analogy table comparing the SKIPS design to the seahorse inspiration, are available here:

https://docs.google.com/document/d/12JfOeIGlDbbYgCg1IYChpOyrqIrz8TJgDMz7KsO9zeA/edit?usp=share_link

## APPENDIX B

SolidWorks CAD models of all final components are available here:

https://drive.google.com/file/d/1mYXa2BEHRsB8ekcpTBYLcppNNoqzkW_q/view?usp=share_link

## APPENDIX C

Complete Arduino code used to control the robot is available here:

https://drive.google.com/drive/folders/1ALy0H1qYzvqhttVX1-CpoF4J0jpT9q5g?usp=share_link

## APPENDIX D

Complete test data, including videos, are available here:

https://drive.google.com/drive/folders/1MmaT0xlbK2KahChW9GhH1XDJJSxcvdSs?usp=share_link

## REFERENCES


[1] S. Aoi, Y. Egi, and K. Tsuchiya, "Instability-based mechanism for body undulations in centipede locomotion," in *Phys. Rev. E*, vol. 87, no. 1, Jan. 2013. doi: 10.1103/PhysRevE.87.012717. [Online]. Available: http://hdl.handle.net/2433/188009

[2] M. A. Simon, S. J. Fusillo, K. Colman, and B. A. Trimmer, "Motor patterns associated with crawling in a soft-bodied arthropod," in *J. Exp. Biol.*, vol. 213, no. 13, pp. 2303-2309, Jul. 2010. doi: 10.1242/jeb.039206. [Online]. Available: https://journals.biologists.com/jeb/article/213/13/2303/34072/Motor-patterns-associated-with-crawling-in-a-soft

[3] S. E. Naleway, J. R. A. Taylor, M. M. Porter, M. A. Meyers, and J. McKittrick, "Structure and mechanical properties of selected protective systems in marine organisms," in *Mater. Sci. Eng.*, vol. 59, pp. 1143-1167, Feb. 2016. doi: 10.1016/j.msec.2015.10.033. [Online]. Available: https://www.sciencedirect.com/science/article/pii/S092849311530463X?pes=vor

[4] M. M. Porter, E. Novitskaya, A. B. Castro-Ceseña, M. A. Meyers, and J. McKittrick, "Highly deformable bones: Unusual deformation mechanisms of seahorse armor," in *Acta Biomaterialia*, vol. 9, no. 6, pp. 6763-6770, Jun. 2013, doi: 10.1016/j.actbio.2013.02.045. [Online]. Available: https://www.sciencedirect.com/science/article/abs/pii/S1742706113001153?via%3Dihub

[5] E. Bruner and V. Bartolino, "Morphological Variation in the Seahorse Vertebral System," in *Int. J. Morphology*, vol. 26, no. 2, pp. 247-262, 2008. doi: 10.4067/S0717-95022008000200002. [Online]. Available: https://www.researchgate.net/publication/234053987_Morphological_Variation_in_the_Seahorse_Vertebral_System

[6] M. M. Porter, D. Adriaens, R. L. Hatton, M. A. Meyers, and J. McKittrick, "Why the seahorse tail is square," in *Science*, vol. 349, no. 6243, Jul. 2015. doi: 10.1126/science.aaa6683.

[7] F. Troya. "Controlling a LED Through Bluetooth® with Nano 33 IoT." Arduino.cc. 2023. [Online]. Available: https://docs.arduino.cc/tutorials/nano-33-iot/bluetooth

[8] G. Eason, B. Noble, and I. N. Sneddon, "On certain integrals of Lipschitz-Hankel type involving products of Bessel functions," Phil. Trans. Roy. Soc. London, vol. A247, pp. 529–551, April 1955.

[9] J. Clerk Maxwell, A Treatise on Electricity and Magnetism, 3rd ed., vol. 2. Oxford: Clarendon, 1892, pp.68–73.

[10] I. S. Jacobs and C. P. Bean, "Fine particles, thin films and exchange anisotropy," in Magnetism, vol. III, G. T. Rado and H. Suhl, Eds. New York: Academic, 1963, pp. 271–350.

[11] K. Elissa, "Title of paper if known," unpublished.

[12] R. Nicole, "Title of paper with only first word capitalized," J. Name Stand. Abbrev., in press.

[13] Y. Yorozu, M. Hirano, K. Oka, and Y. Tagawa, "Electron spectroscopy studies on magneto-optical media and plastic substrate interface," IEEE Transl. J. Magn. Japan, vol. 2, pp. 740–741, August 1987 [Digests 9th Annual Conf. Magnetics Japan, p. 301, 1982].

[14] M. Young, The Technical Writer's Handbook. Mill Valley, CA: University Science, 1989.